Zeitschrift: IABSE publications = Mémoires AIPC = IVBH Abhandlungen
Band: 28 (1968)

Artikel: Inelastic stability of tapered wide-flange columns
Autor: Lin, K.H. / Rossow, E.C. / Lee, S.L.
DOI: https://doi.org/10.5169/seals-22185

Inelastic Stability of Tapered Wide-Flange Columns

Stabilité de colonnes émincées à larges ailes dans le domaine plastique

Stabilität von zugespitzten Breitflanschstützen im plastischen Bereich

K. H. LIN
Ph. D., Associate Senior Research Engineer, General Motors Research Laboratories, Warren, Michigan, U.S.A.

E. C. ROSSOW
Ph. D., Associate Professor of Civil Engineering

S. L. LEE
Ph. D., Professor of Civil Engineering

Northwestern University, Evanston, Illinois, U.S.A.

1. Introduction

The behavior of symmetrically and linearly tapered wide-flange columns made of elastic-plastic materials and subjected to arbitrary end loading which causes bending in addition to axial compression is investigated. The interaction curves for tapered cantilever columns are obtained numerically neglecting any torsional-flexural behavior. Approximate equations for these curves are presented to facilitate the determination of the load carrying capacity of simply supported columns.

Numerous analytical studies have been made of the elastic buckling of axially loaded tapered columns [1–6]. The elastic stability of tapered columns subjected to combined bending and thrust has been treated by several investigators [7–11]. While the inelastic buckling of axially loaded tapered columns has been studied [12–14], little work has been done on the inelastic stability of tapered columns subjected to eccentric loading although columns of uniform cross section under such loading have been analyzed [15–18].

2. Assumptions

The present analysis is based on the following assumptions; the material is elastic-perfectly plastic as shown in Fig. 1; the material is homogeneous and

isotropic in both the elastic and plastic states; plane sections remain plane during bending; deflections, slopes, and curvatures are small and are confined to the plane of the web; the effect of the shear stresses on yielding and curvature is neglected; residual stresses and strain reversal are not considered; instability of snap through type occurs in the plane of web which coincides with the plane of loading; and the idealized section is characterized by an H-shape, where the flange thickness is very small but finite.

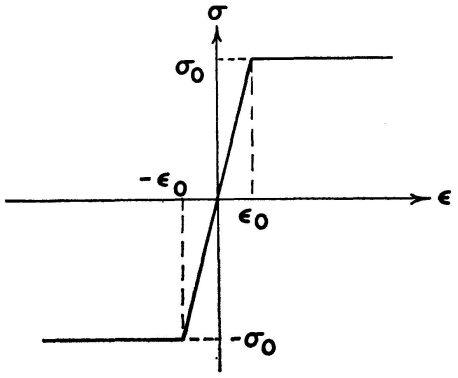

Fig. 1. Idealized stress-strain relationship.

3. Tapered Columns

The column considered herein is symmetrically and linearly tapered along its length by varying the depth of the web but keeping the flange width and thickness constant. The taper slope, denoted by a and defined as the change of the half-depth per unit length of the column, may assume positive or negative values depending on whether the larger or the smaller section is chosen as the reference section. To facilitate the analysis that follows, a rectangular coordinate system is introduced as shown in Fig. 2.

For the reference section where the origin is located, designate the radius of gyration about the strong axis by r_0, the half-depth by b_0, the web area by A_{w0}, and the flange-web area ratio, A_f/A_{w0} by R_0. The nondimensional distance from the origin and the deflection of the centroidal axis are defined respectively, as

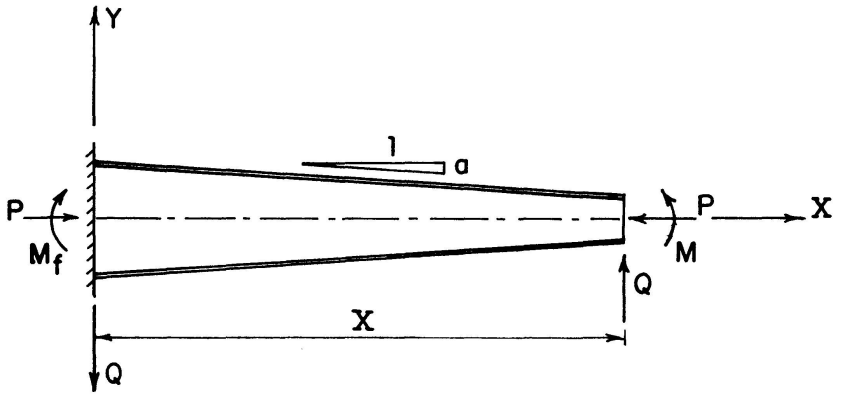

Fig. 2. Tapered wide-flange cantilever column under arbitrary end loads.

$$x = \frac{X}{r_0} \tag{1}$$

and

$$y = \frac{Y}{r_0}. \tag{2}$$

By introducing a parameter

$$\lambda = a\frac{r_0}{b_0}. \tag{3}$$

The following expressions are readily derived for any section.

$$b = b(x) = b_0(1-\lambda x), \tag{4}$$

$$A_w = A_w(x) = A_{w0}(1-\lambda x), \tag{5}$$

$$A = A(x) = A_{w0}(R_0+1-\lambda x), \tag{6}$$

$$R = R(x) = \frac{R_0}{1-\lambda x}, \tag{7}$$

$$I = I(x) = A_{w0}b_0^2(1-\lambda x)^2[R_0+\tfrac{1}{3}(1-\lambda x)], \tag{8}$$

$$S = S(x) = A_{w0}b_0(1-\lambda x)[R_0+\tfrac{1}{3}(1-\lambda x)], \tag{9}$$

$$Z = Z(x) = A_{w0}b_0(1-\lambda x)[R_0+\tfrac{1}{2}(1-\lambda x)], \tag{10}$$

$$r = r(x) = b_0(1-\lambda x)\sqrt{\frac{R_0+\frac{1}{3}(1-\lambda x)}{R_0+1-\lambda x}}, \tag{11}$$

where b, A_w, A, R, I, S, Z and r are respectively, the half-depth, the web area, the total area, the flange-web area ratio, the moment of inertia, the elastic section modulus, the plastic section modulus, and the radius of gyration. Setting $x=0$ in Eq. 11 and substituting into Eq. 3 leads to

$$\lambda = a\sqrt{\frac{R_0+\frac{1}{3}}{R_0+1}}. \tag{12}$$

4. Stress Zones

When a wide-flange section shown in Fig. 3 (a) is subjected to a compressive axial force P and a bending moment M, one of the three stress distributions, referred to as elastic, primary plastic, and secondary plastic, as shown in Figs. 3 (b), (c), and (d) will result.

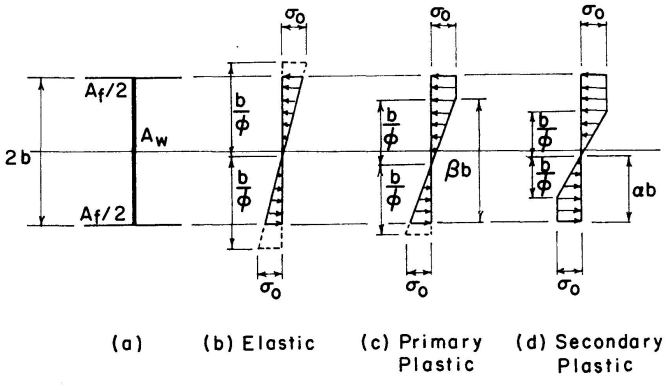

Fig. 3. Cross section and stress distribution due to bending and compression.

The nondimensional axial force and moment are defined, respectively, as

$$p = p(x) = \frac{P}{P_0(x)} \tag{13}$$

and

$$m = m(x) = \frac{M(x)}{M_0(x)}, \tag{14}$$

in which

$$P_0(x) = \sigma_0 A(x) \tag{15}$$

and

$$M_0(x) = \sigma_0 Z(x), \tag{16}$$

where σ_0 denotes the yield stress of the material.

Referring to Fig. 3 (d), the condition $1/\phi = 0$, where ϕ denotes the nondimensional curvature, defines the limit of statical admissibility. The plastic moment is given by

$$m_{pl}(x) = \frac{R_0 + 1 - \lambda x}{R_0 + \frac{1}{2}(1 - \lambda x)}[1 - p(x)] \quad \text{for} \quad \frac{1 - \lambda x}{R_0 + 1 - \lambda x} \leqq p(x) \leqq 1, \tag{17a}$$

$$m_{pl}(x) = 1 - \frac{[(R_0 + 1 - \lambda x)\, p(x)]^2}{(2R_0 + 1 - \lambda x)(1 - \lambda x)} \quad \text{for} \quad 0 \leqq p(x) \leqq \frac{1 - \lambda x}{R_0 + 1 - \lambda x}. \tag{17b}$$

Referring to Fig. 3 (b), the condition of initial yield, which defines the boundary between the elastic and the primary plastic zones, gives

$$m_e(x) = \frac{R_0 + \frac{1}{3}(1 - \lambda x)}{R_0 + \frac{1}{2}(1 - \lambda x)}[1 - p(x)]. \tag{18}$$

The boundary between the primary and the secondary plastic zones is given by the condition $\beta = 2/\phi$ in Fig. 3 (c) and is expressed by

$$m_p = \frac{1}{R_0 + \frac{1}{2}(1 - \lambda x)} \left\{ R_0 + \tfrac{1}{3}(1 - \lambda x) \left[1 + \frac{R_0 + 1 - \lambda x}{1 - \lambda x} p(x) - 2 \left(\frac{R_0 + 1 - \lambda x}{1 - \lambda x} p(x) \right)^2 \right] \right\}. \tag{19}$$

The admissible domain and the boundaries for each stress zone are described by Eqs. 17, 18, and 19 in a p-m plane shown in Fig. 4.

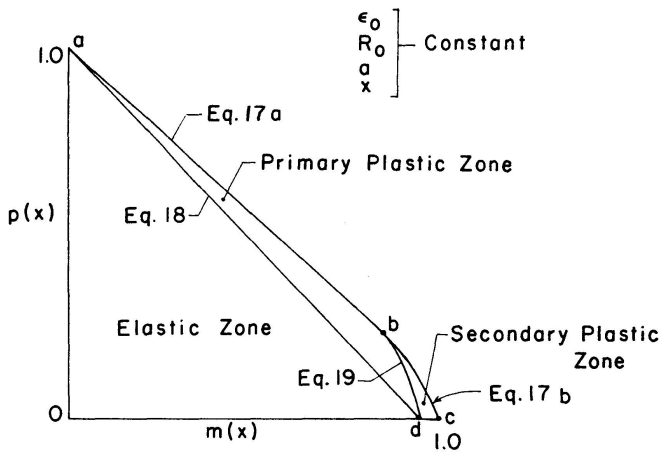

Fig. 4. Stress zones.

5. Curvature Functions

The nondimensional curvature at any section is defined as

$$\phi = \frac{\Phi}{\Phi_0}, \tag{20}$$

where Φ is the actual curvature, $\Phi_0 = \epsilon_0/b$ is the curvature at initial yield due to pure bending, and ϵ_0 is the strain at yield point. The function $\phi(m, p)$ for each stress zone can be readily expressed as follows.

In the elastic zone,

$$\phi = \frac{R_0 + \frac{1}{2}(1-\lambda x)}{R_0 + \frac{1}{3}(1-\lambda x)} m(x), \tag{21}$$

in the primary plastic zone,

$$\phi = \frac{8}{9} \frac{(R_0 + 1 - \lambda x)[1 - p(x)]}{(1-\lambda x)\left\{U\left(U + \frac{2R_0}{1-\lambda x}\right) + \left[U + \frac{2R_0}{3(1-\lambda x)}\right]\sqrt{U\left[U + \frac{8R_0}{3(1-\lambda x)}\right]}\right\}}, \tag{22a}$$

in which

$$U = 1 - \frac{R_0 + \frac{1}{2}(1-\lambda x)}{R_0 + 1 - \lambda x} \frac{m(x)}{1 - p(x)}, \tag{22b}$$

while in the secondary plastic zone,

$$\phi = \frac{1}{\sqrt{3\left\{\frac{2R_0 + 1 - \lambda x}{1-\lambda x}[1 - m(x)] - \left[\frac{R_0 + 1 - \lambda x}{1-\lambda x} p(x)\right]^2\right\}}}. \tag{23}$$

Eqs. (21), (22), and (23) are derived for positive moment, hence the absolute value of m must be used and ϕ replaced by $(-\phi)$ in cases where the moment is negative.

6. Equilibrium Equations

When the tapered cantilever column is subjected to an axial force P, a shear force Q, and a bending moment M at the free end as shown in Fig. 2, the conditions of equilibrium require that

$$m(x) = \frac{1}{[R_0 + \frac{1}{2}(1-\lambda x)](1-\lambda x)}\left[(R_0 + \tfrac{1}{2}) m_f - \sqrt{(R_0+1)(R_0+\tfrac{1}{3})}(p_f y + q_f x)\right], \tag{24}$$

in which $p_f = P/P_0(0)$, $q_f = Q/P_0(0)$, $m_f = M_f/M_0(0)$, and M_f = the fixed end moment. The relation between $p(x)$ and p_f is given by

$$p(x) = \frac{1-\lambda x}{R_0 + 1 - \lambda x} p_f. \tag{25}$$

7. Differential Equation

From the small deflection theory and Eqs. 2 and 20, it follows that

$$\frac{d^2Y}{dX^2} = \frac{1}{r_0}y'' = \frac{\epsilon_0}{b}\phi, \tag{26}$$

in which prime denotes differentiation with respect to x. Introducing Eqs. (3), (4) and (12) in Eq. (26) leads to

$$y'' = \sqrt{\frac{R_0+\frac{1}{3}}{R_0+1}}\,\frac{\epsilon_0}{1-\lambda x}\phi. \tag{27}$$

Substitution of Eqs. (24) and (25) into the appropriate curvature function, i.e., Eq. (21), (22), or (23), and the results into Eq. (27) yields the differential equation for each stress zone.

The boundary conditions

$$y(0) = y'(0) = 0 \tag{28}$$

being both specified at one end of the column make this an initial-value problem.

8. Numerical Integration

The numerical solution of the initial value problem defined by Eqs. (27) and (28) is obtained by a step-by-step integration procedure. Let the subscript i denote the discrete stations evenly spaced along the x-axis such that $x_i = (i-1)\Delta x$, $i = 1, 2, 3\ldots$ Approximating the second derivative in Eq. (27) by a three-term central difference formula, upon application of the boundary conditions, Eq. (28), leads to

$$y_2 = \tfrac{1}{2}\epsilon_0(\Delta x)^2\sqrt{\frac{R_0+\frac{1}{3}}{R_0+1}}\,\phi_1 \tag{29}$$

and in general

$$y_{i+1} = \frac{\epsilon_0(\Delta x)^2}{1-\lambda x_i}\sqrt{\frac{R_0+\frac{1}{3}}{R_0+1}}\,\phi_i + 2y_i - y_{i-1} \quad \text{for } i \geqq 2. \tag{30}$$

For given values of p_f, q_f, and m_f, the values of m_i and p_i can be obtained from Eqs. (24) and (25), respectively. Having determined the stress zone from Eqs. (17), (18), and (19), the appropriate curvature function ϕ_i, Eqs. (21), (22) or (23), is chosen. The value of y_{i+1} can then be computed by means of Eq. (30).

9. Equilibrium Curves

By means of the marching procedure described above, the values of m can be plotted against x for various values of m_f as shown in Fig. 5 (a), provided

the values of ϵ_0, R_0, a, p_f, and q_f are specified. The m-x curves are referred to as equilibrium curves of the tapered cantilever column.

If $|m|$ nowhere exceeds m_e, the column is entirely elastic. In some of the equilibrium curves, $m_e < |m| < m_{pl}$ in a portion of the column. For some values of m_f, the equilibrium curves intersect the curves $m = \pm m_{pl}$ at some point x. Beyond this point, the equilibrium curve is statically inadmissible and need not be considered.

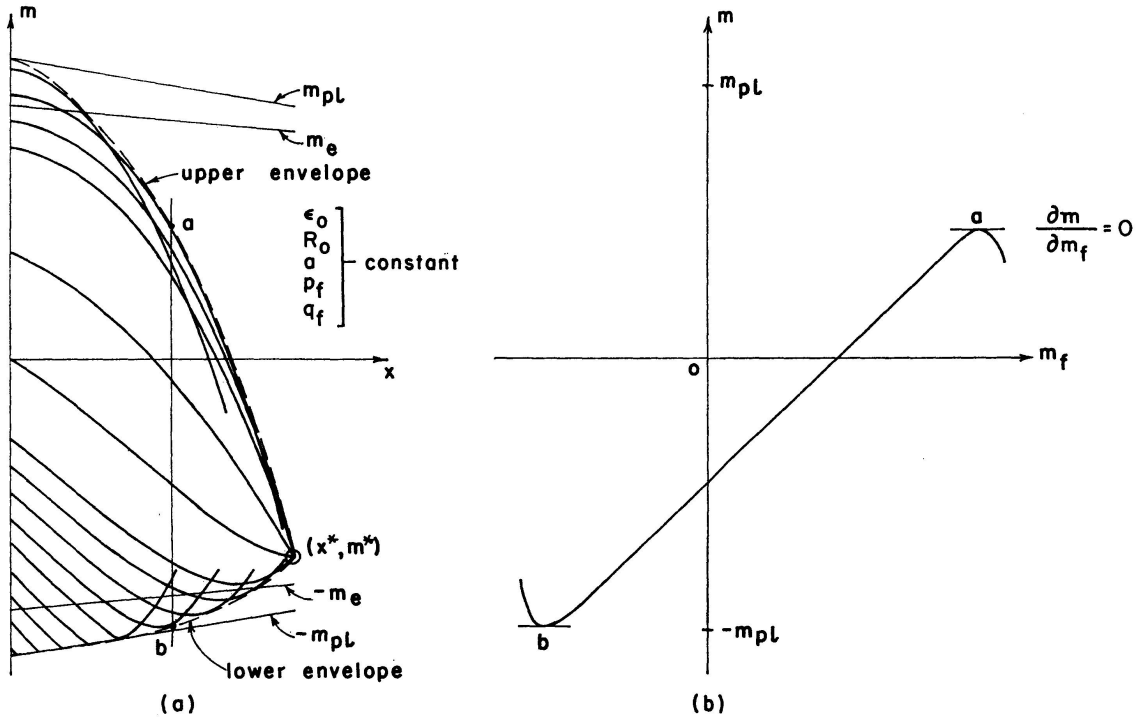

Fig. 5. Moment equilibrium curves and envelopes.

It is of interest to observe that all the elastic equilibrium curves pass through a common point (x^*, m^*). For the inelastic equilibrium curves, the value of x corresponding to m^* are always smaller than x^*. The existence of the common point (x^*, m^*), of the elastic equilibrium curves implies that x^* and m^* are both independent of m_f. If q_f vanishes, all the elastic equilibrium curves meet at $(x^*, 0)$. Thus, x^* is the nondimensional elastic buckling length or Euler length.

10. Elastic Tapered Columns

Elasting Buckling Length x^*. Consider an elastic cantilever column subjected to an axial force P at the free end. The differential equation for the centroidal axis of the slightly bent column is

$$(C_1 x^3 + C_2 x^2 + C_3 x + C_4) y'' + C_5 y = C_5 \delta, \tag{31}$$

in which $C_1=\lambda^3$, $C_2=-3\lambda^2(R_0+1)$, $C_3=3\lambda(2R_0+1)$, $C_4=-(3R_0+1)$, $C_5=-(3R_0+1)$, $\epsilon_0 p_f$ and δ is the arbitrary deflection at the free end. The boundary conditions are

$$y(0) = 0, \tag{32a}$$

$$y'(0) = 0, \tag{32b}$$

$$y(x^*) = \delta. \tag{32c}$$

Examining the coefficient function of Eq. (31) indicates that $x=0$ is an ordinary point and $x=(3R_0+1)/\lambda$ and $x=1/\lambda$ are both regular singular points. The complementary function takes the form of an infinite power series which converges uniformly for $0 \leqq x < |1/\lambda|$.

Taking the solution of the boundary value problem defined by Eqs. (31) and (32) in the form $y=\delta+\sum_{k=0}^{\infty} a_k x^k$ and demanding the nontrivial solution lead to the elastic buckling criterion

$$\sum_{k=0}^{\infty} a_k (x^*)^k = 0, \tag{33}$$

in which

$$a_0 = -\delta, \tag{34a}$$

$$a_1 = 0, \tag{34b}$$

$$a_2 = -\frac{C_5}{2C_4}, \tag{34c}$$

$$a_k = -\frac{1}{k(k-1)C_4}\{a_{k-1}(k-1)(k-2)C_3 + a_{k-2}[(k-2)(k-3)C_2 + C_5] + a_{k-3}(k-3)(k-4)C_1\}, \qquad k = 3, 4, 5, \ldots \tag{34d}$$

For a given value of p_f, the smallest positive real root x^* of Eq. (33) is the elastic buckling length of the cantilever column.

The Euler length x^* can also be obtained with excellent accuracy by intersecting any elastic equilibrium curve for $q_f=0$ with the x-axis by means of the numerical integration procedure. It must be pointed out that if $a<0$, the Euler length is obtainable from Eq. (33) for $x^*<|1/\lambda|$, whereas the numerical solution is always valid. The x^*-p_f curves for various taper slopes are presented in solid lines in Fig. 6.

Determination of m^*. Consider the cantilever column subjected to general loading at the free end as shown in Fig. 2. Assuming that the column is entirely elastic, the differential equation may be obtained by combining Eqs. (21), (24), and (27) as

$$(C_1 x^3 + C_2 x^2 + C_3 x + C_4) y'' + C_5 y = C_5 \left[\frac{2R_0+1}{2\sqrt{(R_0+1)(R_0+\frac{1}{3})}}\left(\frac{m_f}{p_f}\right) - \left(\frac{q_f}{p_f}\right)x\right]. \tag{35}$$

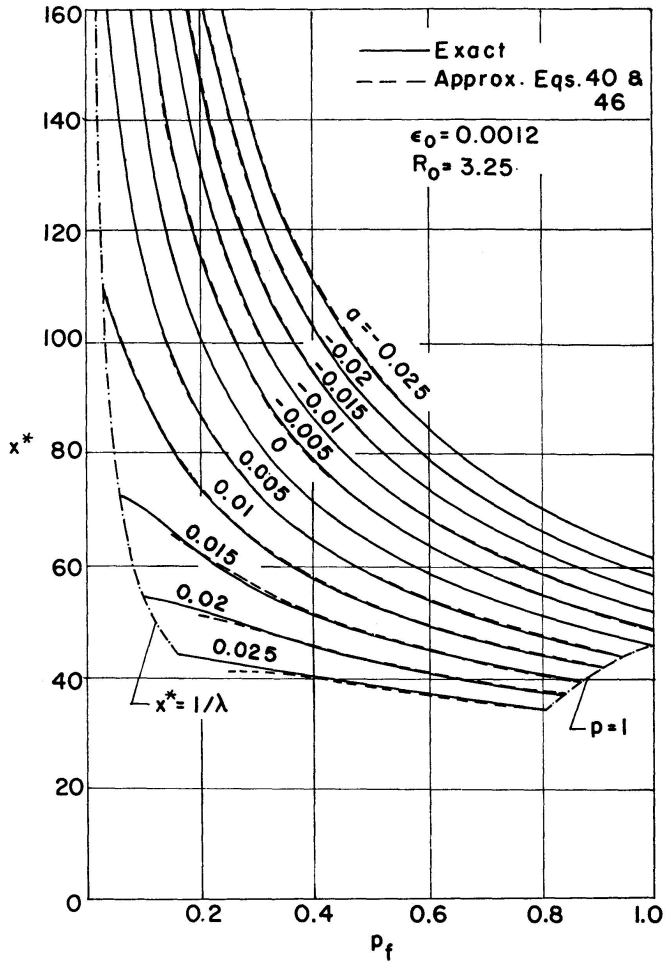

Fig. 6. Euler lengths of tapered cantilever columns.

The boundary conditions are

$$y(0) = 0, \tag{36a}$$

$$y'(0) = 0. \tag{36b}$$

The homogeneous equation corresponding to Eq. (35) is identical to that corresponding to Eq. (31).

Solving the initial value problem defined by Eqs. (35) and (36) and substituting the solution into Eq. (24) leads to the equation of the elastic equilibrium curve

$$m(x) = \frac{1}{[R_0 + \frac{1}{2}(1-\lambda x)](1-\lambda x)} \{(R_0+\tfrac{1}{2})\, m_f - \sqrt{(R_0+1)(R_0+\tfrac{1}{3})}\, p_f \sum_{k=1}^{\infty} c_k x^k\}, \tag{37}$$

in which

$$c_0 = -\frac{2R_0+1}{2\sqrt{(R_0+1)(R_0+\frac{1}{3})}} \left(\frac{m_f}{p_f}\right), \tag{38a}$$

$$c_1 = \frac{q_f}{p_f}, \tag{38b}$$

$$c_2 = \frac{(2R_0+1)\epsilon_0}{4\sqrt{(R_0+1)(R_0+\frac{1}{3})}} m_f, \tag{38c}$$

$$c_k = -\frac{1}{k(k-1)C_4}\{c_{k-1}(k-1)(k-2)C_3 + c_{k-2}[(k-2)(k-3)C_2 + C_5] + c_{k-3}(k-3)(k-4)C_1\}, \qquad k = 3, 4, 5, \ldots \tag{38d}$$

Since the common point (x^*, m^*) of elastic equilibrium curves is independent of m_f, it is appropriate to set $m_f = 0$ in Eqs. (37) and (38) to obtain the expression for m^* in the form

$$m^* = m(x^*) = -\frac{\sqrt{(R_0+1)(R_0+\frac{1}{3})}}{[R_0+\frac{1}{2}(1-\lambda x^*)](1-\lambda x^*)} p_f \sum_{k=1}^{\infty} c_k (x^*)^k. \tag{39}$$

It is important to observe that the coefficients, $c_k, k = 1, 2, 3, \ldots$, hence m^* are linear functions of q_f.

The expression for m^* given by Eq. (39) is valid only when $x^* < |1/\lambda|$. However, the value of m^* can always be obtained numerically as the value of m for any elastic curves at $x = x^*$. The $m^* - p_f$ curves for various taper slopes are presented in solid lines for a particular value of q_f as shown in Fig. 7. The values of m^* for other values of q_f can be obtained by linear proportioning.

Insensitivity of x^* and m^* to R_0. It is observed that the values of x^* and m^* are insensitive to the variation of the parameter R_0. The following approximate expressions for x^* and m^* are derived on the basis of $R_0 = 3.25$.

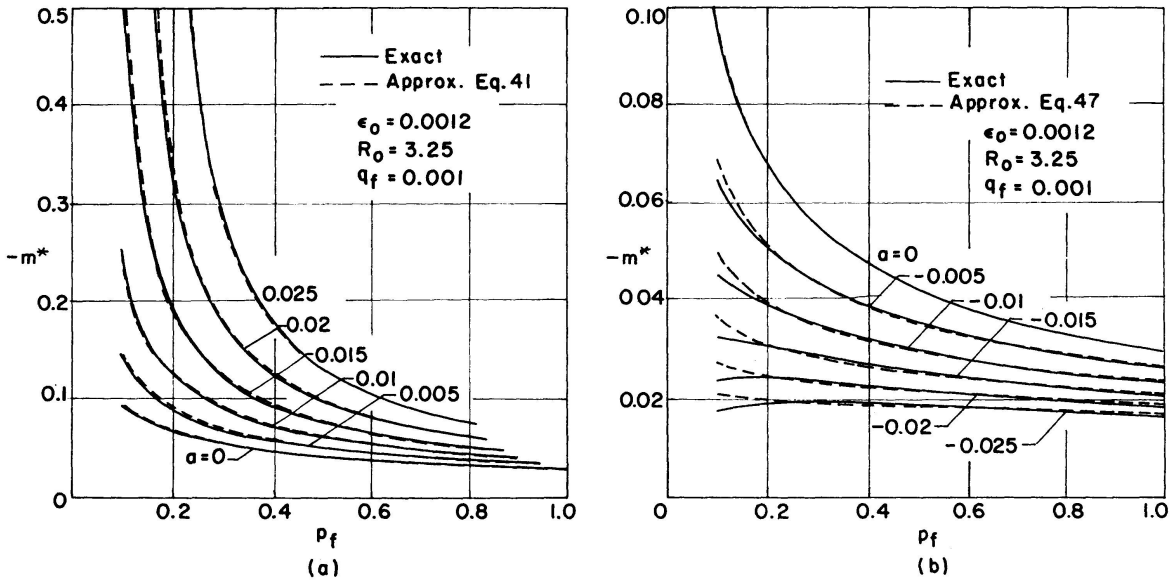

Fig. 7. Variation of m^* with p_f and a.

11. Approximate Expressions for x^* and m^*

The values of x^* and m^* for $R_0 = 3.25$ and $\epsilon_0 = 0.0012$, corresponding to A 36 steel, for taper slopes in the range $-0.025 \leqq a \leqq 0.025$ may be approximated by the following expressions.

For $0 \leqq a \leqq 0.025$,

$$x^* = \frac{\pi}{\sqrt{0.0048\, p_f}} - \frac{481.1\, a^{0.9647}}{p_f^{[0.9953/(10^{1.14\, a})]}}, \tag{40}$$

$$m^* = -q_f \{10^{[\alpha_m/(p_f^{\beta_m})-6]} + \Delta_m H(p_{fc} - p_f)\}, \tag{41}$$

in which

$$\left.\begin{aligned} \alpha_m &= 7.480 + 9.20\, a \\ \beta_m &= 0.02816 + 1.495\, a \end{aligned}\right\} \text{ for } 0 \leqq a \leqq 0.0125 \tag{42a, 42b}$$

$$\left.\begin{aligned} \alpha_m &= 7.414 + 14.50\, a \\ \beta_m &= 0.03229 + 1.165\, a \end{aligned}\right\} \text{ for } 0.0125 \leqq a \leqq 0.025 \tag{43a, 43b}$$

$$\Delta_m = \frac{(a/0.015)^{7.85}}{(p_f/0.30)^{5.32}}, \tag{44}$$

$$p_{fc} = -0.2625 + 32.5\, a \tag{45}$$

and H denotes the Heaviside unit function, i.e., $H(\eta) = 0$ for $\eta < 0$ and $H(\eta) = 1$ for $\eta > 0$.

For $-0.025 \leqq a \leqq 0$

$$x^* = \frac{\pi}{\sqrt{0.0048\, p_f}} + \frac{688.1\, (-a)^{1.027}}{p_f^{[1.007/(10^{0.587\, a})]}}, \tag{46}$$

$$m^* = -q_f \times 10^{[\alpha_m/(p_f^{\beta_m})-6]}, \tag{47}$$

in which

$$\left.\begin{aligned} \alpha_m &= 7.469 + 9.20\, a \\ \beta_m &= 0.02695 + 0.867\, a \end{aligned}\right\} \text{ for } -0.025 \leqq a \leqq -0.0125 \tag{48a, 48b}$$

$$\left.\begin{aligned} \alpha_m &= 7.480 + 10.10\, a \\ \beta_m &= 0.02816 + 0.964\, a \end{aligned}\right\} \text{ for } -0.0125 \leqq a \leqq 0 \tag{49a, 49b}$$

The approximate Euler lengths obtained from Eqs. (40) and (46) are plotted as dashed lines in Fig. 6. The approximate values of m^* obtained from Eqs. (41) and (47) are plotted as dashed lines in Fig. 7. It is seen that, in both cases, the approximation is satisfactory for practical purposes.

12. Interaction Curves

For a given set of ϵ_0, R_0, a, p_f, and q_f, a family of equilibrium curves, as shown in Fig. 5 (a), can be constructed. From this family of curves, an $m - m_f$ curve can be plotted for a given value of x such as shown in Fig. 5 (b). At point a or b where the slope of the $m - m_f$ curve vanishes, i.e.,

$$\frac{\partial m}{\partial m_f} = 0 \tag{50}$$

the column is in the state of neutral equilibrium. Thus, Eq. (50) defines the limit of stability and is used as the inelastic stability criterion. The loci of all maximum points such as a and minimum points such as b corresponding to different values of x represent, respectively, the upper and lower envelopes

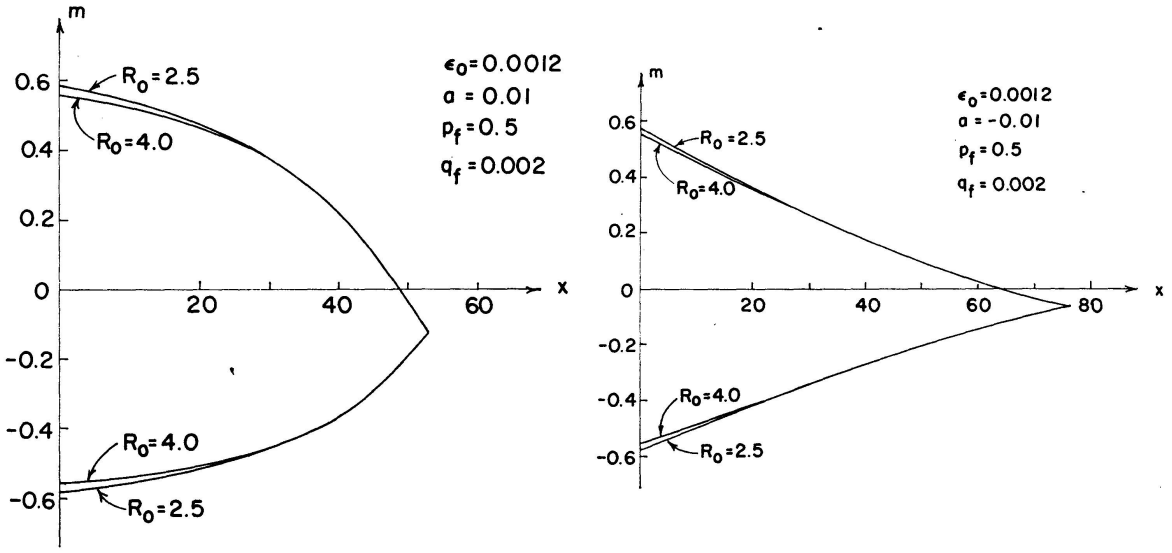

Fig. 8. Influence of R_0 on interaction curves.

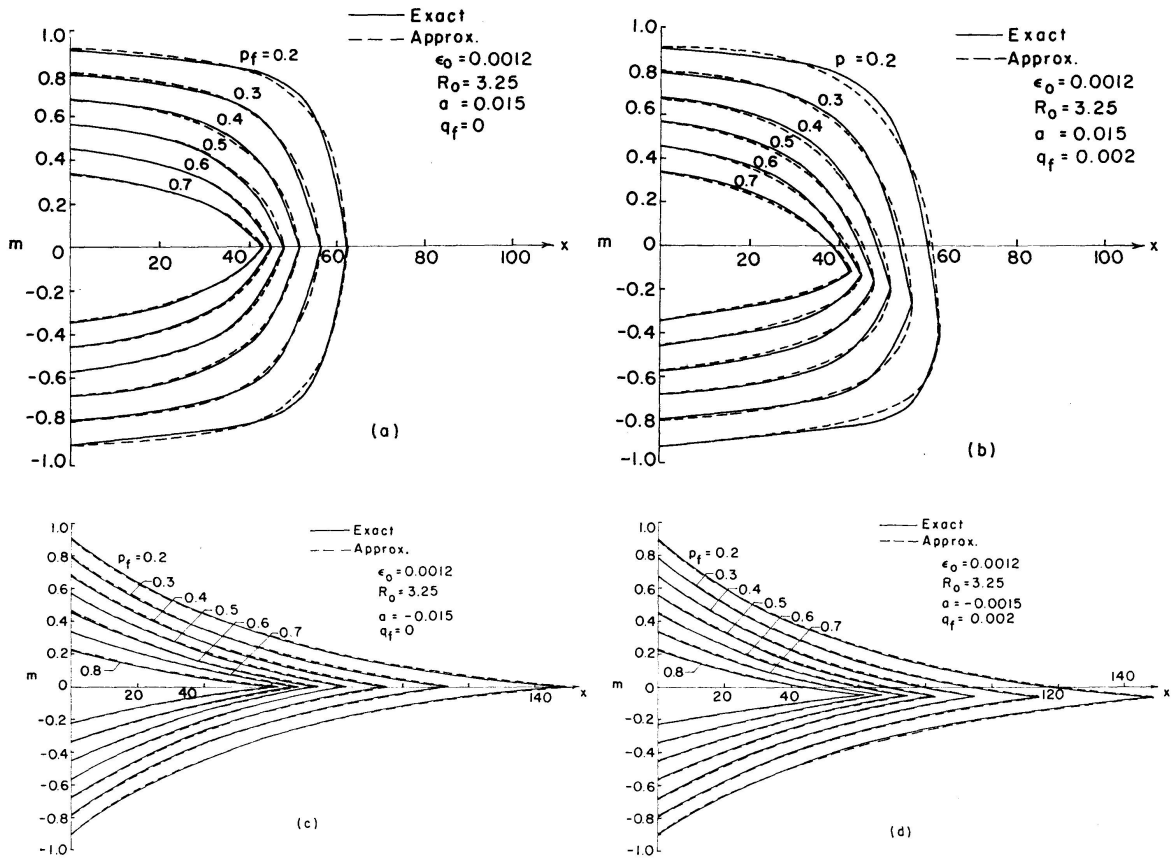

Fig. 9. Interaction curves.

of the family of equilibrium curves as shown in Fig. 5 (a). The envelopes are referred to as interaction curves and define the ultimate strength of the tapered cantilever column under various end loading conditions.

It is found that the interaction curve is insensitive to the parameter R_0 as shown in Fig. 8. Typical interaction curves are presented in Fig. 9.

Let q_f^* and q_f^{**} be the values of q_f which satisfy, respectively,

$$m^* = -m_e^*, \tag{51}$$

$$m^* = -m_{pl}^*, \tag{52}$$

where m_e^* and m_{pl}^* are, respectively, the values of m_e and m_{pl} at $x=x^*$. The $q_f^*-p_f$ and $q_f^{**}-p_f$ curves for various taper slopes are shown in Fig. 10.

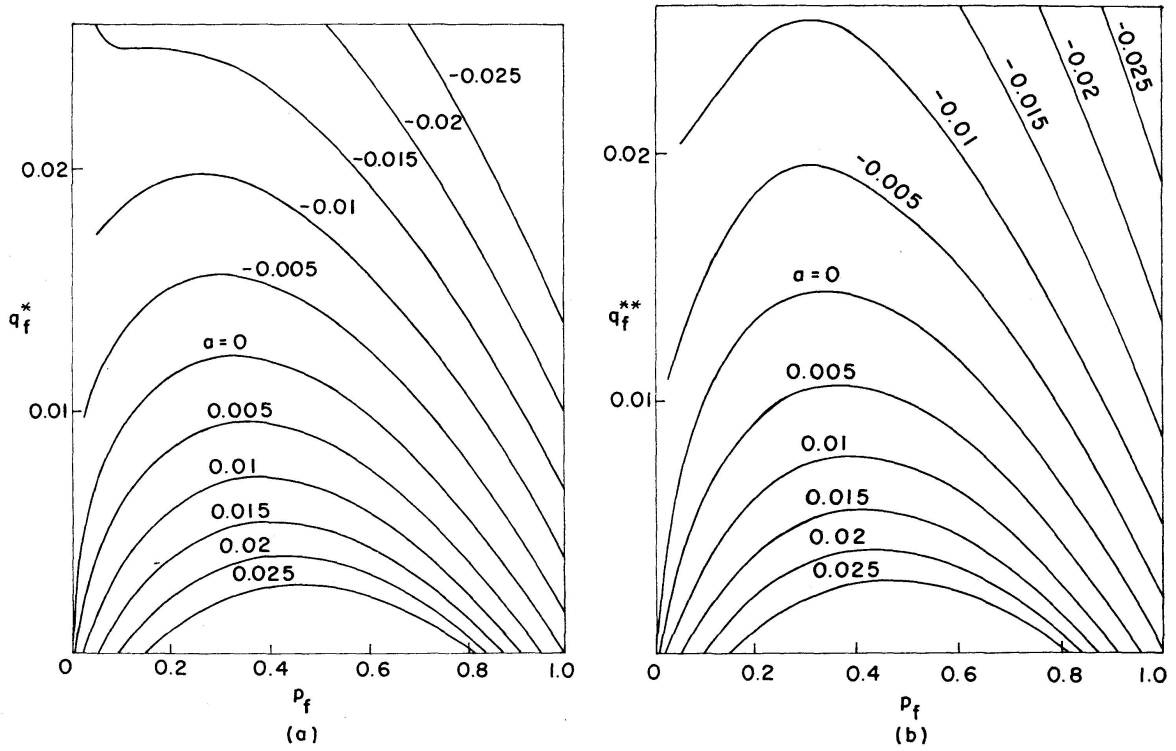

Fig. 10. q_f^* and q_f^{**}—p_f curves.

The intersection of the upper and lower envelopes is the same as the common point (x^*, m^*) of the elastic equilibrium curves as long as $q_f \leqq q_f^*$. When q_f exceeds q^*, neither the elastic equilibrium curve nor the common point exists. However, the numerical value of m^* can still be computed as if the column were infinitely elastic. For $q_f^* < q_f \leqq q_f^{**}$, it can be shown that the point (x^*, m^*) still defines the intersection of the envelopes.

For $q_f \geqq q_f^*$, the $-m_{pl}(x)$ curve, which is independent of q_f, completely governs the lower envelope and the intersection, denoted by (x^{**}, m^{**}), shifts along the lower envelope toward the negative x-direction as q_f increases. Therefore, the maximum admissible length x^{**} is smaller than the Euler length x^*. The computed (x^*, m^*), which lies outside of the admissible domain,

will be used in the next section as a fictitious end point of the upper envelope for obtaining approximate interaction equations. The point (x^{**}, m^{**}) can be located numerically by intersecting the upper and lower envelopes.

13. Approximate Interaction Equation

The actual interaction curves constructed for $R_0 = 3.25$ and $\epsilon_0 = 0.0012$ for taper slopes in the ranges $0.005 \leqq |a| \leqq 0.025$ may be approximated by the following expressions.

The upper envelope is approximated by

$$m = \overline{m} + (m^* - \overline{m})\,\xi + \mu\,[10 - 10\,(a - 0.01)\,H\,(a - 0.01)] \tag{53}$$

and the lower envelope by

$$m = -\overline{m} + (m^* + \overline{m})\,\xi + \mu\,[10 - 10\,(a - 0.01)\,H\,(a - 0.01)] \quad \text{for } 0 \leqq q_f \leqq q_f^{**}, \tag{54a}$$

$$m = -\overline{m} + (m_{pl}^* + \overline{m}) \quad \text{for } q_f \geqq q_f^{**}, \tag{54b}$$

in which $\overline{m} = m_{pl}(0)$, $m_{pl}^* = m_{pl}(x^*)$, $\xi = x/x^*$, x^* is obtained from Eq. (40) or Eq. (46), m^* from Eq. (41) or Eq. (47) and

$$\left.\begin{aligned} \mu &= C\,\bar{\xi}\,(1 - \bar{\xi}^2)^n && (55a)\\ n &= \frac{(1 - \bar{\xi}^2)}{2\,\bar{\xi}^2} && (55b)\\ C &= \frac{\bar{\mu}}{\bar{\xi}\,(1 - \bar{\xi}^2)^n} && (55c) \end{aligned}\right\} \quad \text{for } \bar{\xi} \geqq 0.5,$$

$$\left.\begin{aligned} \mu &= C\,(1 - \xi)\,(2\,\xi - \xi^2)^n && (56a)\\ n &= \frac{2\,\bar{\xi} - \bar{\xi}^2}{2\,(1 - \bar{\xi})^2} && (56b)\\ C &= \frac{\bar{\mu}}{(1 - \bar{\xi})\,(2\,\bar{\xi} - \bar{\xi}^2)^n} && (56c) \end{aligned}\right\} \quad \text{for } \bar{\xi} \leqq 0.5.$$

The new variables $\bar{\xi}$ and $\bar{\mu}$ in Eqs. (55) and (56) are functions of a, p_f, and q_f and defined as follows:

For $0.005 \leqq a \leqq 0.025$,

$$\bar{\xi} = 0.5254 \times 10^{[8.31\,a + (p_f - 0.4)\,\psi_1]} - (23\,p_f + 7)\,q_f, \tag{57}$$

$$\bar{\mu} = 3.743\,a^{0.6057} - (p_f - 0.4)\,\psi_2 + 1641000\,a^{2.685}\,(2\,p_f)^{-\sqrt{3}}\,q_f \tag{58}$$

for the upper envelope, and

$$\bar{\xi} = 0.5254 \times 10^{[8.31\,a + (p_f - 0.4)\,\psi_1]} + [22 - 38.44 \times 10^{-35.43\,a} + (p_f - 0.4)\,\psi_3]\,q_f, \tag{59}$$

$$\bar{\mu} = -3.743\,a^{0.6057} - (p_f - 0.4)\,\psi_2 + 8.464 \times 10^{48.74\,a}\,(2.5\,p_f)^{\psi_4}\,q_f \tag{60}$$

for the lower envelope, in which

$$\psi_1 = 0.4354\,a^{-0.1401} - 1 \qquad \text{for } p_f \leqq 0.4, \tag{61a}$$

$$\psi_1 = -4.242\,a^{0.9247} \qquad \text{for } p_f \geqq 0.4, \tag{61b}$$

$$\psi_2 = -21.47\,a^{0.6888} \qquad \text{for } p_f \leqq 0.4 \text{ and } a \leqq 0.02, \tag{62a}$$

$$\psi_2 = -1.45 \qquad \text{for } p_f \leqq 0.4 \text{ and } a \geqq 0.02, \tag{62b}$$

$$\psi_2 = -17.48\,a^{0.785} \qquad \text{for } p_f \geqq 0.4, \tag{62c}$$

$$\psi_3 = -35 \qquad \text{for } p_f \leqq 0.4, \tag{63a}$$

$$\psi_3 = -15 \qquad \text{for } p_f \geqq 0.4, \tag{63b}$$

$$\psi_4 = -0.931 \times 10^{15.49\,a} \qquad \text{for } p_f \geqq 0.4, \tag{64a}$$

$$\psi_4 = -0.2644 \times 10^{27.67\,a} \qquad \text{for } p_f \geqq 0.4. \tag{64b}$$

For $-0.025 \leqq a \leqq -0.005$

$$\bar{\xi} = 0.1012\,(-a)^{-0.3544} \times 10^{(p_f - 0.4)\psi_5} + (1.4 - 15\,p_f)\,q_f, \tag{65}$$

$$\bar{\mu} = \psi_6 - 6.705\,p_f^{-0.4949}\,q_f \tag{66}$$

for the upper envelope, and

$$\bar{\xi} = 0.1012\,(-a)^{-0.3544} \times 10^{(p_f - 0.4)\psi_5} + [0.0153\,(-a)^{-1.75\,b}\,p_f^{1.337} - 1]\,q_f, \tag{67}$$

$$\bar{\mu} = \psi_6 - 6.705\,p_f^{-0.4949}\,q_f \tag{68}$$

for the lower envelope, in which

$$\psi_5 = 0.2 - 5\,a \qquad \text{for } p_f \leqq 0.4, \tag{69}$$

$$\psi_5 = 0.1875 \qquad \text{for } p_f \geqq 0.4, \tag{70}$$

$$\psi_6 = 11.52\,(-a)^{0.7619} \times 10^{-0.3745\,(-a)^{-0.331}\,p_f} \qquad \text{for } p_f \leqq 0.6, \tag{71a}$$

$$\psi_6 = 11.52\,(-a)^{0.7619} \times 10^{-[0.2247(-a)^{-0.331} + 2\,p_f - 1.2]} \qquad \text{for } p_f \geqq 0.6. \tag{71b}$$

The curves defined by Eqs. (53) and (54) are plotted in dashed lines alongside the actual interaction curves in Fig. 9 and show reasonably close approximation. Being insensitive to the parameter R_0, the interaction curves in Fig. 9 or the approximate expressions given by Eqs. (53) and (54) may be applied for practical purposes to tapered wide-flange cantilever columns made of A 36 steel for $2.5 \leqq R_0 \leqq 4.0$.

In the case where q_f exceeds q_f^{**}, the intersection of the upper and lower envelopes, i.e., (x^{**}, m^{**}), is readily located by solving Eqs. (53) and (54b) simultaneously.

It should be pointed out that the interaction equations presented above do not apply for the range $-0.005 < a < 0.005$. In practice, tapered columns in this range are hardly used.

14. Simply Supported Columns

The approximate interaction equations, Eqs. (53) and (54), derived for cantilever columns can be extended to the treatment of the simply supported tapered column shown in Fig. 11 (a). The column is subjected to axial force P

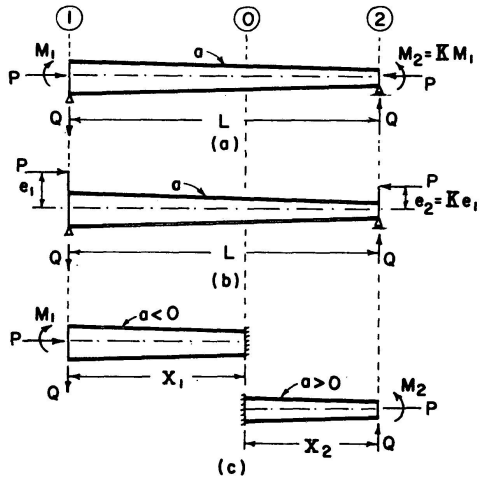

Fig. 11. Simply supported tapered columns.

and unequal end moments M_1 and M_2 where $M_2 = K M_1$, for $-1 \leqq K \leqq 1$. The simply supported column of length L may be considered as two cantilever columns of lengths X_1 and X_2 with the fixed end located at section 0 as shown in Fig. 11 (c). The taper slopes of the two cantilever columns are of the same magnitude but of opposite sign and the fixed end is taken as the reference section.

Referring to Fig. 11 (c), the right segment X_2 is subjected to the same type of loading as the cantilever column of Fig. 2. However, the shear force Q acting on the left segment X_1 is opposite in sense to that shown in Fig. 2. Therefore, the corresponding interaction curves for the left segment must be turned upside down as shown in Fig. 12 where the x_1-axis is directed toward the left for convenience in the combined $m - x_1$ and $m - x_2$ planes.

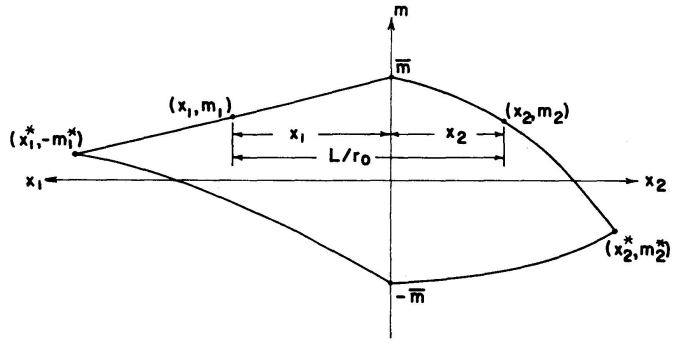

Fig. 12. Interaction curves for a simply supported tapered column.

The values of x_1 and x_2 at the point where the column becomes unstable are not known *a priori*. However, the relation

$$x_1 + x_2 = \frac{L}{r_0} \tag{72}$$

must hold true and the points (x_1, m_1) and (x_2, m_2) must both lie on the interaction curves. In other words, the solution of the stability problem is reduced to solving three simultaneous algebraic equations by a trial-and-error procedure outlined in the following.

Suppose p_1 and K are specified for a given column, and the critical value of m_1 is to be determined. Referring to Fig. 11, let R_1 and r_1 be the flange-web area ratio and the radius of gyration, respectively, of section 1 and $\lambda_1 = a\sqrt{(R_1+1/3)/(R_1+1)}$ in which a assumes a positive value. A trial reference section 0 is located by assuming a value of X_1/r_1. The relation

$$\left(\frac{r_1}{r_0}\right) = \frac{\sqrt{\frac{R_1+\frac{1}{3}}{R_1+1}}}{\frac{R_1+\frac{1}{3}\left[1-\lambda_1\left(\frac{X_1}{r_1}\right)\right]}{\sqrt{R_1+1-\lambda_1\left(\frac{X_1}{r_1}\right)}}\left[1-\lambda_1\left(\frac{X_1}{r_1}\right)\right]} \tag{73}$$

is readily established in view of Eq. (11), and x_1 and x_2 are then obtained, respectively, from

$$x_1 = \left(\frac{X_1}{r_1}\right)\left(\frac{r_1}{r_0}\right), \tag{74a}$$

$$x_2 = \left(\frac{L}{r_1} - \frac{X_1}{r_1}\right)\left(\frac{r_1}{r_0}\right). \tag{74b}$$

The nondimensional axial force with reference to section 0 is given by

$$p_f = \frac{R_1+1}{R_1+1-\lambda_1\left(\frac{X_1}{r_1}\right)} p_1. \tag{75}$$

Knowing p_f, the corresponding x^* for the right and left segments are computed, respectively, from Eqs. (40) and (46). The value of m^*_{pl} for each segment are obtained from Eq. (41) or (47).

Next assume a trial value of m_1, corresponding to which

$$m_2 = \kappa m_1 \tag{76a}$$

where

$$\kappa = \frac{(R_1+\frac{1}{2})}{\left\{R_1+\frac{1}{2}\left[1-\lambda_1\left(\frac{L}{r_1}\right)\right]\right\}\left[1-\lambda_1\left(\frac{L}{r_1}\right)\right]} K, \tag{76b}$$

the nondimensional shear force is given by

$$q_f = \frac{m_1}{\left(\frac{L}{r_1}\right)} \frac{(R_1+\frac{1}{2})(1-K)}{\sqrt{\frac{R_1+\frac{1}{3}}{R_1+1}}\left[R_1+1-\lambda_1\left(\frac{X_1}{r_1}\right)\right]}. \tag{77}$$

The value of m^*, which is a function of q_f, for the right segment is obtained from Eq. (41). In the case where $m^* < -m^*_{pl}$, the intersection of the upper and lower envelopes, (x^{**}, m^{**}), must be computed by the method described in Section 13. For the left segment, m^* corresponding to Q acting in the direction opposite to that shown in Fig. 11 (c) is obtained from Eq. (47).

Table 1. Classification of Interaction Equations

Case	Left Segment, $a<0$, $x=x_1$			Right Segment, $a>0$, $x=x_2$	
1a 1b 1c 1d	$0 \leqq q_f \leqq q_f^{**}$ i. e., $0 \geqq m^* \geqq -m_{pl}^*$	$m_1 \geqq -m^*$ $m_1 \leqq -m^*$	Eqs. 54a, 67, 68 Eqs. 53, 65, 66	$0 \leqq q_f \leqq q_f^{**}$ i. e., $0 \geqq m^* \geqq -m_{pl}^*$	$m_2 \geqq m^*$ Eqs. 53, 57, 58 $m_2 \leqq m^*$ Eqs. 54a, 59, 60 $m_2 \geqq m^*$ Eqs. 53, 57, 58 $m_2 \leqq m^*$ Eqs. 54a, 59, 60
2a 2b 2c 2d	$0 \leqq q_f \leqq q_f^{**}$ i. e., $0 \geqq m^* \geqq -m_{pl}^*$	$m_1 \geqq -m^*$ $m_1 \leqq m^* \leqq m_{pl}^*$	Eqs. 54a, 67, 68 Eqs. 53, 65, 66	$q_f \geqq q_f^{**}$ i. e., $m^* \leqq -m_{pl}^*$	$m_2 \geqq m^{**}$ Eqs. 53, 57, 58 $m_2 \leqq m^{**}$ Eqs. 54b $m_2 \geqq m^{**}$ Eqs. 53, 57, 58 $m_2 \leqq m^{**}$ Eqs. 54b

Note: m is replaced by $-m$ when Eqs. 53 and 54 are applied to the left segment.

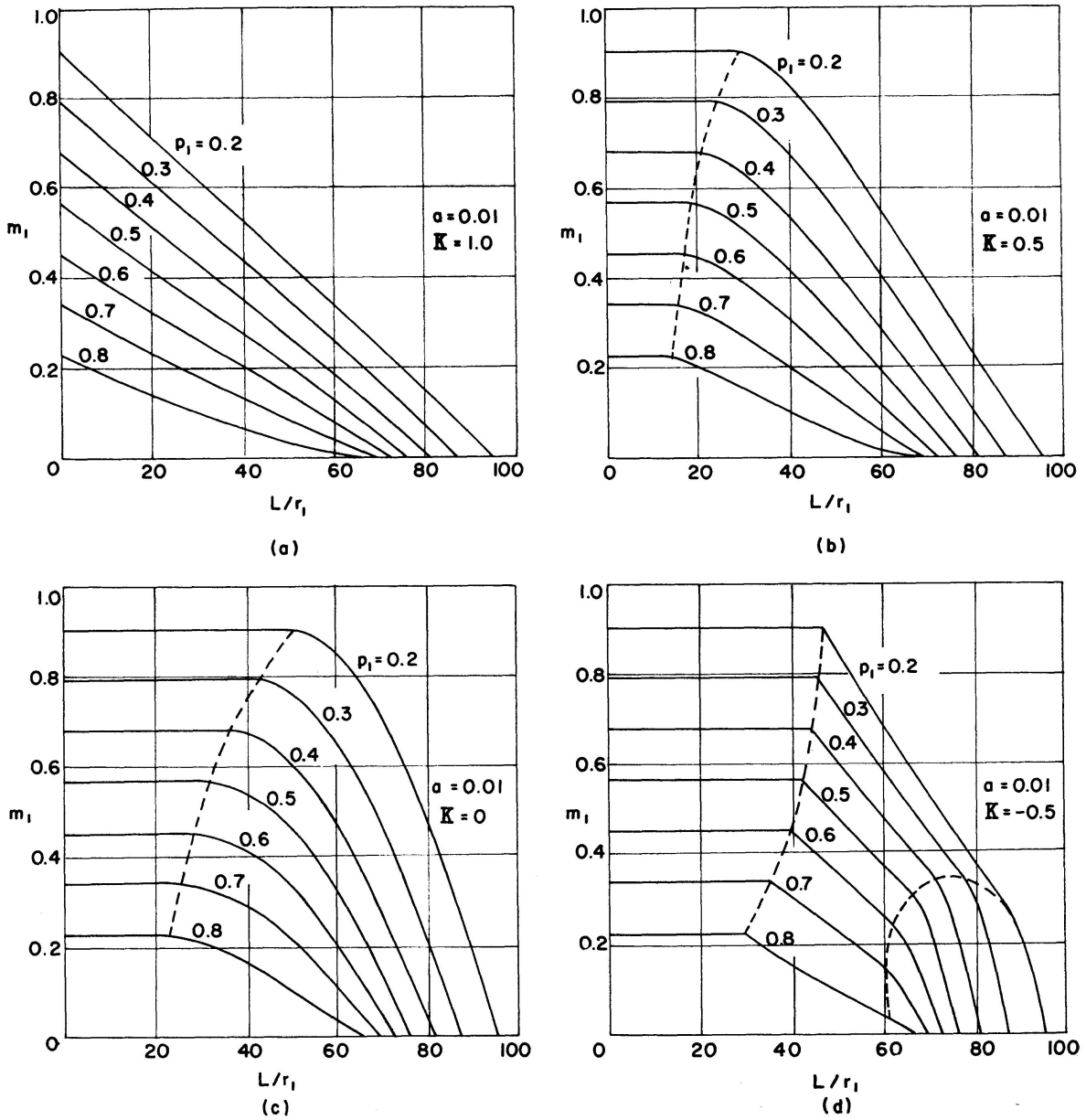

Fig. 13. Column curves (A 36 steel).

The value of q_f determines which set of the approximate interaction curves is to be used for the solution of a given problem. Two cases, each contains four subcases, thus arise and are listed in Table 1.

Once the appropriate set of interaction equations is chosen for the particular case listed in Table 1, the values of the interaction curves at x_1 and x_2 can be computed and compared with the trial values of m_1 and m_2, respec-

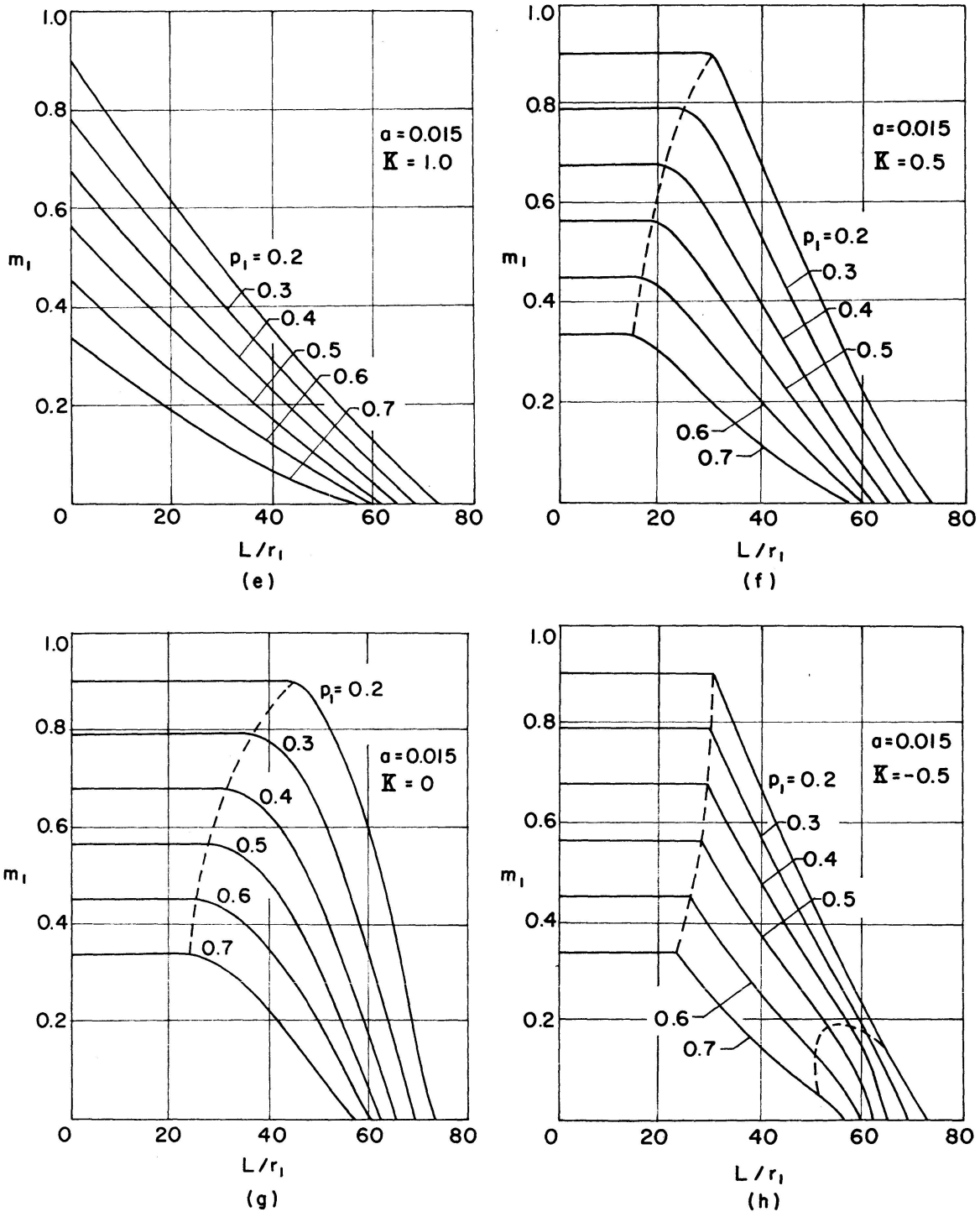

Fig. 13. Column curves (A 36 steel).

tively. The trial value of m_1 is varied until the interaction equation for each segment is satisfied. However, the two interaction equations may not be satisfied for the same trial value of m_1. It is necessary to vary the trial value of X_1/r_1 and to repeat the above-mentioned process until both interaction equations are satisfied simultaneously. The corresponding value of m_1 gives the critical end moment.

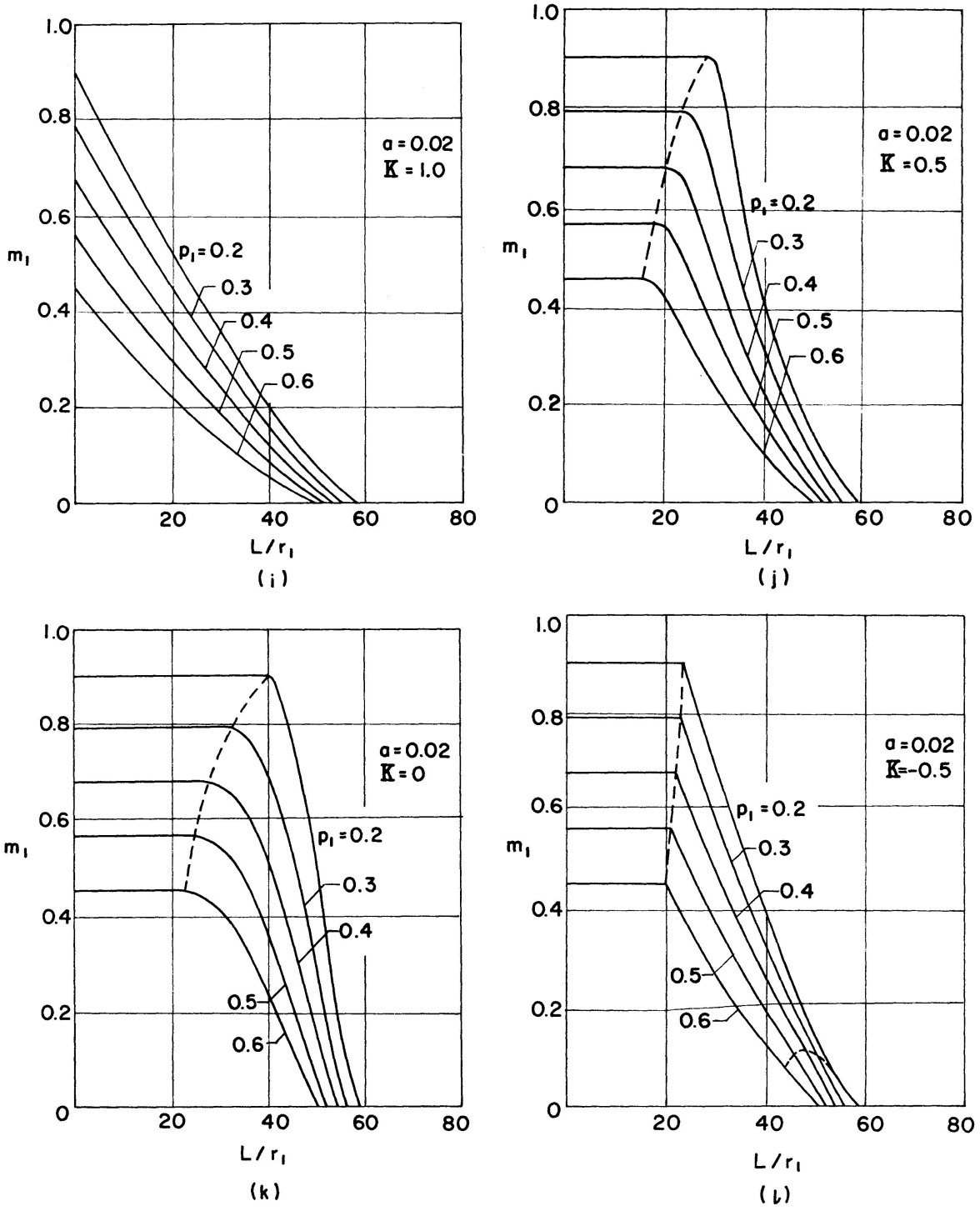

Fig. 13. Column curves (A 36 steel).

The trial-and-error procedure described above, taking into account all the cases shown in Table 1, is built into a computer program.

15. Column Curves

Column curves, i.e., $m_1 - L/r_1$ curves, are prepared for A 36 steel in Fig. 12 for various combinations of the parameters a, p_1, and K. These curves can be used to solve for ultimate loads of A 36 steel wide-flange columns subjected to various end loading conditions.

It is of interest to observe that for the case where $K = 1$, i.e., Figs. 13 (a), (e), and (i), the carrying capacity of the columns is governed entirely by instability. For $0 \leqq K < 1$, the ultimate load carrying capacity is governed either by yielding of the large end section for short columns or by instability for longer columns, and the demarcation line between these two regions is shown by the dashed line in Figs. 13 (b), (c), (f), (g), (j) and (k). When $K < 0$, there are three different regions, separated by the dashed lines shown in Fig. 13 (d), (h), and (l), representing, from left to right, yielding of the large end section, yielding of the small end section, and instability.

16. Illustrative Examples

A few examples illustrating the use of the approximate interaction equations as well as the column curves are given in the following.

Example 1. A tapered wide-flange cantilever column made of A 36 steel is loaded as shown in Fig. 2. Find the critical values of the applied end moment m if $L/r_0 = 35$, $R_0 = 3.25$, $a = 0.015$, $p_f = 0.5$, and $q_f = 0.002$.

Eqs. (40) and (41) give, respectively, $x^* = 47.88$ and $m^* = -0.1586$. Setting $x = 0$ in Eq. (17a) yields $\overline{m} = 0.5667$ and, referring to Fig. 10, it is found that $0 < q_f < q_f^{**}$ in this case.

Upper limit: Substituting a, p_f, and q_f into Eqs. (57) and (58) give $\bar{\xi} = 0.6491$ and $\bar{\mu} = 0.2710$ for which $n = 0.6866$ is obtained from Eq. (55b) and $C = 0.6079$ from Eq. (55c). Substituting $\xi = 35/47.88$ into Eq. (55a) gives $\mu = 0.2629$. Finally Eq. (53) yields $m = 0.2863$ which is the upper limit of m.

Lower limit: Substituting a, p_f, and q_f into Eqs. (59) and (60) give $\bar{\xi} = 0.7045$ and $\bar{\mu} = -0.1513$, respectively, for which $n = 0.5073$ is obtained from Eq. (55b) and $C = -0.3041$ from Eq. (55c). Substituting $\xi = 35/47.88$ into Eq. (55a) yields $\mu = -0.1508$. Finally, Eq. (54a) yields $m = -0.4117$, which is the lower limit of m.

As long as $-0.4117 < m < 0.2863$, the column is stable. The values obtained from the actual interaction curves, Fig. 9 (b), are $-0.422 < m < 0.304$.

Example 2. A tapered wide-flange column made of A 36 steel is simply supported and eccentrically loaded as shown in Fig. 11 (b). Find the critical

value of p_1 at which the column passes from stable to unstable equilibrium if $L/r_1 = 40$, $R_1 = 2.5$, $a = 0.015$, $e_2/e_1 = 0.5$. and $e_1' = e_1 A_1/Z_1 = m_1/p_1 = 0.8$.

From Fig. 13 (f), an $m_1 - p_1$ curve for $L/r_1 = 40$ is constructed as shown in Fig. 14. The solution is obtained by intersecting this curve with the straight line $m_1 = 0.8\, p_1$. This gives $p_1 = 0.442$ as the critical value for which $m_1 = p_1 e_1' = 0.3536$.

Using $p_1 = 0.442$ in solving the approximate interaction equations for m_1, by means of the trial-and-error procedure described in Section 14, yields $m_1 = 0.3547$ which verifies the graphical solution.

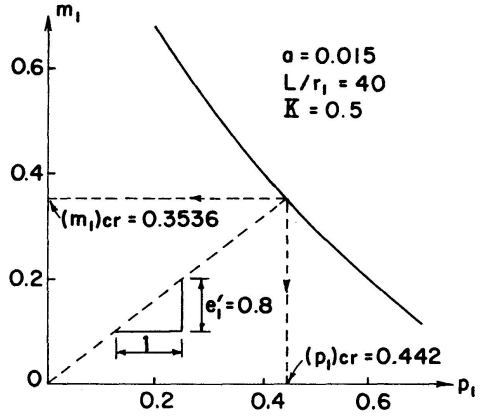

Fig. 14. Graphical solution of example 2.

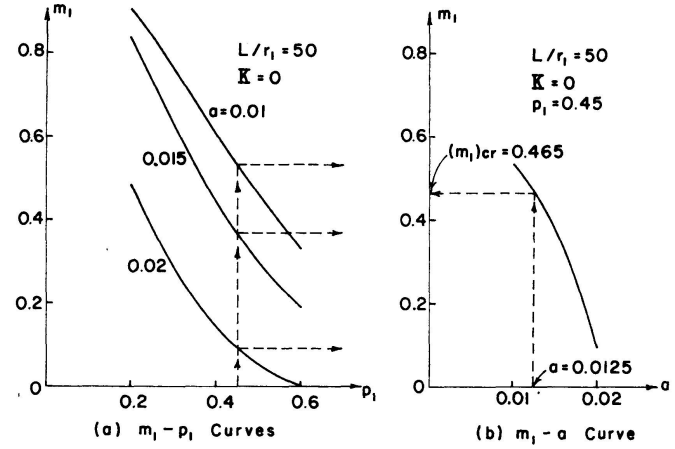

Fig. 15. Graphical solution of example 3.

Example 3. A simply supported tapered wide-flange column made of A 36 steel, as shown in Fig. 11 (a), is subjected to the end moment at the left end in addition to the axial force, i. e., $K = 0$. Find the maximum value of the end moment for which the column remains stable if $L/r_1 = 50$, $R_1 = 2.5$, $a = 0.0125$, and $p_1 = 0.45$.

From Figs. 13 (c), (g), and (k), the $m_1 - p_1$ curves for $L/r_1 = 50$ are plotted for three different values of a as shown in Fig. 15 (a). From these curves, read off the values of m_1 at $p_1 = 0.45$ and plot them against a as shown in Fig. 15 (b) from which $m_1 = 0.465$ is obtained for $a = 0.0125$. The value obtained from the approximate interaction equations is $m_1 = 0.472$.

17. Conclusions

The method presented above leads to a more realistic evaluation of the strength of tapered columns than is possible either from a consideration of elastic behavior only, or from the elementary treatment of columns concentrically loaded into the plastic range.

The curvature functions, expressed in closed form, are also valid for box sections provided the stress-strain relationship and cross sections are idealized the same way.

The excellent agreement between the exact solution and the numerical solution for x^* and m^* assures the applicability of the latter which is straightforward and less time-consuming. It is observed that the interaction curves are insensitive to the parameter R_0. For practical purposes, $R_0 = 3.25$ is used to derive the approximate interaction equations. It schould be pointed out that for materials other than A 36 steel, the approximate expressions must be rederived.

The carrying capacity of simply supported columns is governed by inelastic instability, yielding at the large end, or yielding at the small end depending on the combination of the parameters a, K and p_1.

With appropriate modifications in the formulations, the present method can be extended to investigate the inelastic stability of columns of nonlinear taper, or elastic-strain hardening materials.

18. References

1. Dinnik, A. N.: Design of Columns of Varying Cross Section. Transactions, ASME, Vol. 51, APM-51-11, 1929, p. 105—114, and Vol. 54, APM-54-16, 1932, p. 165—171.
2. Timoshenko, S. P., and Gere, J. M.: Theory of Elastic Stability. 2nd ed., McGraw-Hill Book Co., Inc., New York, 1961, p. 125—132.
3. Nakagawa, H.: Buckling of Columns with Tapered Part. Transactions, Japan Society of Mechanical Engineers, Vol. 3, No. 11, May, 1937, p. 111—119.
4. Miesse, C. C.: Determination of the Buckling Load for Columns of Variable Stiffness. Transactions, ASME, Vol. 71, 1949, p. 406—410.
5. Bleich, F.: Buckling Strength of Metal Structures. McGraw-Hill Book Co., Inc., New York, 1952, p. 186—192.
6. Gere, J. M. and Carter, W. O.: Critical Buckling Loads for Tapered Columns. Journal of the Structural Division, ASCE, Vol. 88, No. ST 1, Proc. Paper 3045, February, 1962, p. 1—11.
7. Gatewood, B. E.: Buckling Loads for Beams of Variable Cross Section under Combined Loads. Journal of the Aeronautical Sciences, Vol. 22, No. 4, April, 1955, p. 281—282.
8. Fogel, C. M. and Ketter, R. L.: Elastic Strength of Tapered Columns. Journal of the Structural Division, ASCE, Vol. 88, No. ST 5, Proc. Paper 3301, October 1962, p. 67—106.
9. Bulter, D. J. and Anderson, G. B.: The Elastic Buckling of Tapered Beam-Columns. Welding Journal, Vol. 42, 1963, p. 29-S—36-S.
10. Lee, G. C. and Kawai, T.: Elastic Stability of Tapered Members. Civil Engineering Project Report No. 44, Department of Civil Engineering, State University of New York at Buffalo, Buffalo, N. Y., April, 1967.
11. Culver, C. G. and Preg, S. M., Jr.: Elastic Stability of Tapered Beam-Columns. Journal of the Structural Division, ASCE, Vol. 94, No. ST 2, Proc. Paper 5796, February, 1968, p. 455—470.
12. Young, D. H.: Inelastic Buckling of Variable Section Columns. Transactions, ASME, Vol. 67, 1945, p. A-166-169.
13. Goldberg, J. E., Bogandoff, J. L. and Lo, H.: Inelastic Buckling of Nonuniform Columns. Transactions, ASCE, Vol. 122, 1957, p. 722—730.

14. Appl, F. J. and Smith, J. O.: Buckling of Inelastic, Tapered, Pin-Ended Columns. Journal of the Engineering Mechanics Division, ASCE, Vol. 94, No. EM 2, Proc. Paper 5897, April, 1968, p. 549—558.
15. Horne, M. R.: The Elastic-Plastic Theory of Compression Members. Journal of the Mechanics and Physics of Solids, Vol. 4, 1956, p. 104—120.
16. Hauck, G. F. and Lee, S. L.: Stability of Elasto-Plastic Wide-Flange Columns. Journal of the Structural Division, ASCE, Vol. 89, No. St 6, Proc. Paper 3738, December, 1963, p. 297—324.
17. Lee, S. L. and Hauck, G. F.: Buckling of Steel Columns under Arbitrary End Loads. Journal of the Structural Division, ASCE, Vol. 90, No. ST 2, Proc. Paper 3872, April, 1964, p. 179—200.
18. Lee, S. L. and Anand, S. C.: Buckling of Eccentrically Loaded Steel Columns. Journal of the Structural Division, ASCE, Vol. 93, No. ST 2, Proc. Paper 4796, April, 1967, p. 351—370.

Summary

The stability of symmetrically and linearly tapered wide-flange columns made of elastic-plastic materials and subjected to combined bending and axial loads is investigated. Torsional-flexural behavior is not considered. Approximate interaction equations are derived for cantilever columns. These interaction equations are used to determine the load carrying capacity of simply supported columns subjected to arbitrary end loading conditions. Column curves for A 36 steel are prepared. Numerical examples are given to illustrate the use of the approximate interaction equations as well as the column curves.

Résumé

Des études de stabilité sous sollicitation combinée flexion-compression ont été faites sur des colonnes émincées symétriquement et linéairement, à larges ailes et en un matériau élastoplastique. Les effets de torsion de flexion ont été négligés. Pour les colonnes encastrées, on a développé des équations d'interaction approximées, qui servent à déterminer la charge de rupture de colonnes simples, soumises à des conditions de charge arbitraires. Des courbes pour colonnes en acier A 36 sont en préparation. Des valeurs numériques sont données pour illustrer l'emploi des équations et des courbes.

Zusammenfassung

Symmetrisch und linear verjüngte Breitflanschstützen aus elastoplastischem Material wurden unter einer gleichzeitigen Biege- und Druckbeanspruchung auf ihre Stabilität untersucht. Das Biegedrillverhalten wurde dabei nicht berücksichtigt. Für eingespannte Stützen wurden Näherungsgleichungen entwickelt, mit deren Hilfe man die Bruchlast von einfachen Stützen für beliebige Lastfälle bestimmen kann. Diagramme für Stützen aus Stahl A 36 sind in Vorbereitung. Es wurden numerische Werte gegeben, um den Gebrauch der Gleichungen und der Diagramme zu veranschaulichen.